ELSEVIER

Journal of Alloys and Compounds 452 (2008) 234–240

Journal of ALLOYS AND COMPOUNDS

www.elsevier.com/locate/jallcom

Structural and magnetic properties of the $(Ca_{1-x}Na_x)(Fe_{2-x}Ti_x)O_4$ solid solution $(0 \leq x \leq 1)$

S. Zouari [a,b], L. Ranno [b], A. Cheikh-Rouhou [a], O. Isnard [b], P. Wolfers [b], P. Bordet [b], P. Strobel [b,*]

[a] *Laboratoire de Physique des Matériaux, Faculté des Sciences de Sfax, B.P. 763, 3038 Sfax, Tunisia*
[b] *Institut Néel, CNRS and Université Joseph Fourier, B.P. 166, 38042 Grenoble, Cedex 9, France*

Received 25 November 2006; received in revised form 11 January 2007; accepted 12 January 2007
Available online 19 January 2007

Abstract

New compounds corresponding to the $(Ca_{1-x}Na_x)(Fe_{2-x}Ti_x)O_4$ formula with $0 \leq x \leq 1$ were prepared by solid state reactions at 1100 °C in air. A continuous solid solution was found between end members $CaFe_2O_4$ and $NaFeTiO_4$. The evolution of structural parameters and bonding geometry with composition is discussed in detail. Magnetic measurements show that the antiferromagnetic ordering known in $CaFe_2O_4$ is suppressed for all x values investigated ($x \geq 0.2$). The absence of crystallographic transition at low temperature was checked by X-ray diffraction down to 10 K. The magnetic structure of $CaFe_2O_4$ was redetermined from powder neutron diffraction. Spins on the two iron sites order antiparallel (F_zF_z spin arrangement), as described previously. The difference in magnetic moments on Fe_1 and Fe_2 sites result in a ferrimagnetic configuration with net moment $2.72\mu_B$ at 2 K.
© 2007 Elsevier B.V. All rights reserved.

Keywords: Oxide materials; Crystal structure; Magnetic measurements; Neutron diffraction

1. Introduction

Calcium ferrite, $CaFe_2O_4$, crystallizes in an orthorhombic structure, space group *Pnma*, containing two iron octahedral sites Fe_1 and Fe_2. The structure is made up of distorted FeO_6 octahedra sharing edges and corners, and eight-fold coordinated calcium atoms [1,2]. This structure type (or distorted variants of it) is encountered not only in various CaM_2O_4 phases (M = Ti, V, Mn), but also in sodium compounds with charge distribution $NaM^{3+}M'^{4+}O_4$; examples are known with B = Sc, Fe and B′ = Ti, Sn [3]. The crystal structures of all these phases belong to the same space group (*Pbnm*) as $CaFe_2O_4$.

$CaFe_2O_4$ is known to exhibit a ferrimagnetic structure below $T_C = 160$ K [4,5]. The spin arrangement was determined in the 60 s [4,5]. It is characterized by an antiparallel alignment of Fe_1 and Fe_2 spins along the *b*-axis in *Pnma* setting [5] (the older literature often used a *Pbnm* cell with a different axis setting). In view of this interesting magnetic structure, and of the structural similarity between the calcium and sodium phases, we undertook a study of the solid solution $(1-x)CaFe_2O_4$, $xNaFeTiO_4$, or $(Ca_{1-x}Na_x)(Fe_{2-x}Ti_x)O_4$.

In this paper, we report the synthesis, structural and magnetic study of this solid solution, which is found to exist in the whole concentration range $(0 \leq x \leq 1)$. Magnetic measurements will show that $CaFe_2O_4$ is the only compound in the series showing magnetic ordering: this feature is suppressed for titanium substitution levels as low as 10% ($x = 0.2$). The crystal and magnetic structure of $CaFe_2O_4$ was redetermined from X-ray and neutron diffraction data at low temperature.

2. Experimental

Powder samples of $CaFe_2O_4$ and $NaFeTiO_4$ were synthesized by a conventional solid-state ceramic method starting from stoichiometric mixtures of $CaCO_3$, $NaCO_3$, TiO_2 and Fe_2O_3 (>99.9% purity). The starting materials are mixed in an agate mortar and fired in air repeatedly at 1200 °C in air with intermediate regrindings.

Members of the $(Ca_{1-x}Na_x)(Fe_{2-x}Ti_x)O_4$ solid solution were obtained using the end members $CaFe_2O_4$ and $NaFeTiO_4$ as precursors. Mixtures in appropriate proportions were pressed into pellets and fired in air, initially at

* Corresponding author at: Institut Néel-Cristallographie, CNRS, B.P. 166, 38042 Grenoble, Cedex 9, France.
E-mail address: pierre.strobel@grenoble.cnrs.fr (P. Strobel).

0925-8388/$ – see front matter © 2007 Elsevier B.V. All rights reserved.
doi:10.1016/j.jallcom.2007.01.074

1000 °C, then twice at 1100 °C for 48 h, with intermediate regrinding and furnace cooling.

Phase purity, homogeneity, and unit cell dimensions were determined by powder X-ray diffraction with a Bruker D8 diffractometer equipped with a Kevex Si(Li) solid detector and Cu Kα radiation and operating in transmission geometry. Intensities were recorded from 11° to 91° 2θ with a 0.025 2θ step and 80 s counting time per step. A rotating sample holder was used to minimize preferential orientation effects.

Magnetization measurements were performed using an extraction magnetometer in the temperature range of 10–300 K. Studies of magnetization as a function of applied field were carried out up to 8 T.

In order to determine the magnetic structure, neutron diffraction experiments were carried out at Institut Laue-Langevin (Grenoble, France), using the high flux D1B diffractometer (position sensitive detector of 400 cells). Patterns were collected at 0.02° intervals of 2θ from 24.00° to 88.00° using a wavelength of 2.52 Å at 2k steps in the temperature range of 1.5–300 K. An additional diffractogram was recorded with 1.28504 Å at 280 K in order to collect a larger number of reflections for structure refinement.

Because of the small number of reflections available in the neutron diffraction study, an additional X-ray powder thermodiffraction study was carried out, in order to check for possible distortion at low temperature. This was achieved in the temperature range of 3–470 K using a bath cryostat with kapton windows mounted on a high-resolution diffractometer operating in Bragg-Brentano focus-

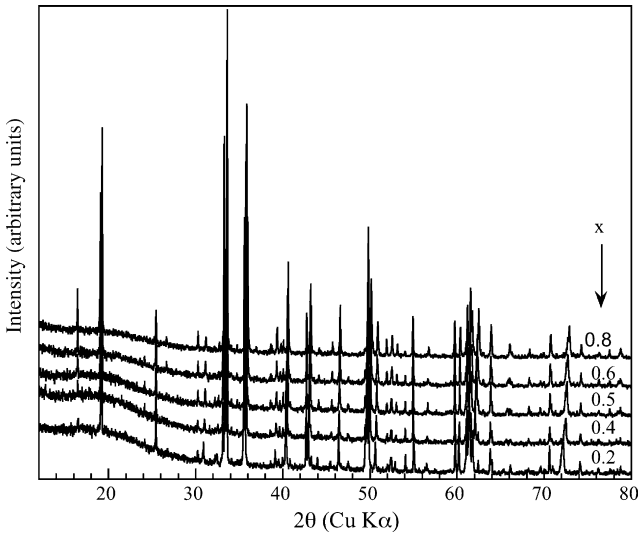

Fig. 1. XRD patterns of $(Ca_{1-x}Na_x)(Fe_{2-x}Ti_x)O_4$ compounds with various values of x.

Table 1
Results of Rietveld refinements along the $CaFe_2O_4$–$NaFeTiO_4$ solid solution (from XRD data at room temperature)

		x						
		0	0.2	0.4	0.5	0.6	0.8	1
Cell parameters (Å)								
a		9.922 (1)	9.2116 (9)	9.2019 (8)	9.1974 (6)	9.1930 (5)	9.1852 (4)	9.1695 (8)
b		3.017 (1)	3.0004 (3)	2.9870 (3)	2.9806 (2)	2.9758 (2)	2.9678 (2)	2.9627 (2)
c		10.689 (2)	10.724 (1)	10.7382 (9)	10.7413 (7)	10.7428 (6)	10.7453 (4)	10.7355 (9)
Positional and thermal parameters (all atoms in 4c position, $y = 1/4$)								
Ca(Na)	x	0.2373 (20)	0.2418 (11)	0.2429 (14)	0.2442 (11)	0.2427 (9)	0.2431 (7)	0.2403 (23)
	z	0.3440 (14)	0.3447 (10)	0.3452 (13)	0.3453 (10)	0.3458 (8)	0.3450 (6)	0.3514 (24)
	B (Å^2)	1.56 (75)	0.08 (23)	0.37 (30)	0.49 (23)	1.37 (20)	1.78 (18)	1.75 (56)
$Fe_1(Ti_1)$	x	0.0846 (18)	0.0826 (8)	0.0844 (10)	0.0846 (7)	0.0840 (6)	0.0851 (4)	0.0839 (12)
	z	0.6090 (12)	0.6057 (7)	0.6056 (9)	0.6054 (6)	0.6050 (4)	0.6046 (3)	0.6065 (11)
	B (Å^2)	1.18 (39)	0.53 (22)	0.63 (26)	0.52 (19)	1.46 (15)	1.25 (11)	1.19 (32)
$Fe_2(Ti_2)$	x	0.0724 (21)	0.0658 (8)	0.0654 (9)	0.0648 (6)	0.0648 (5)	0.0634 (4)	0.0630 (10)
	z	0.1116 (13)	0.1117 (6)	0.1093 (8)	0.1102 (5)	0.1103 (4)	0.1111 (3)	0.1107 (11)
	B (Å^2)	0.93 (39)	0.06 (22)	0.07 (25)	−0.01 (18)	0.89 (13)	0.83 (11)	0.22 (30)
O_1	x	0.2970 (64)	0.2886 (28)	0.2849 (32)	0.2849 (24)	0.2881 (16)	0.2922 (12)	0.2841 (34)
	z	0.6687 (90)	0.6648 (25)	0.6585 (31)	0.6567 (23)	0.6557 (14)	0.6529 (11)	0.6522 (33)
	B (Å^2)	0.75 (36)	1[a]	1[a]	1[a]	1[a]	1[a]	1[a]
O_2	x	0.3769 (39)	0.3841 (26)	0.3819 (30)	0.3851 (22)	0.3832 (15)	0.3848 (11)	0.3828 (31)
	z	−0.0242 (45)	0.9776 (26)	0.9751 (29)	0.9722 (21)	0.9775 (15)	0.9807 (12)	0.9778 (30)
	B (Å^2)	0.75 (36)	1[a]	1[a]	1[a]	1[a]	1[a]	1[a]
O_3	x	0.4740 (63)	0.4775 (31)	0.4815 (35)	0.4789 (25)	0.4776 (17)	0.4758 (14)	0.4799 (38)
	z	0.2142 (48)	0.2199 (25)	0.2190 (29)	0.2207 (21)	0.2196 (14)	0.2171 (12)	0.2158 (31)
	B (Å^2)	0.75 (36)	1[a]	1[a]	1[a]	1[a]	1[a]	1[a]
O_4	x	0.0823 (51)	0.0835 (28)	0.0840 (32)	0.0802 (24)	0.0813 (16)	0.0781 (13)	0.0741 (36)
	z	−0.0654 (39)	0.9205 (22)	0.09240 (26)	0.9243 (19)	0.9236 (13)	0.9252 (10)	0.9274 (24)
	B (Å^2)	0.75 (36)	1[a]	1[a]	1[a]	1[a]	1[a]	1[a]
Statistical parameters								
N–P + C		4270	3108	3120	3076	3152	3138	2891
R_{wp}		0.725	14.2	13.2	13.3	11.8	11.1	9.91
R_{exp}		0.37	10.19	10.11	10.48	8.34	8.91	9.36
χ^2		3.88	1.96	1.71	1.61	2	1.56	1.12
R_{Bragg}		13.1	8.23	8.2	8.86	6.63	4.48	6.29

Space group *Pnma*.
[a] Not refined.

ing geometry (primary beam focusing quartz monochromator, Cr $K\alpha_1$ radiation) [6].

The nuclear and magnetic structures were analyzed with the Rietveld method using the Fullprof [7] and MXD [8] software programs, respectively.

3. Results and discussion

3.1. Solid solution and crystallographic structure

Fig. 1 shows the evolution of the X-ray patterns as a function of Ti content x. All patterns are indexable in space group *Pnma*; no impurity lines were detected. The cell parameters are given in Table 1 (upper part). The simultaneous substitution of iron by titanium and of calcium by sodium leads to a monotonous decrease of a and b cell parameters (see Fig. 2). On the contrary, c initially increases up to a maximum value for $x \approx 0.8$, then decreases slightly on the titanium-rich side (see Fig. 2c). The overall evolution corresponds to a small (1.9%) cell volume decrease (see Fig. 2d). It should be noted that this double substitution corresponds to rather small ion size changes between the pairs Fe^{3+} (0.64 Å)–Ca^{2+} (1.00 Å) and Ti^{4+} (0.605 Å)–Na^{+} (1.02 Å), according to Shannon's octahedral radii scale [9].

The crystal structures of all solid solution members were refined using the Rietveld method. Each atom lies in position 4*c*: x, 1/4, z in the *Pnma* space group. Table 1 summarizes the refinement results and includes final atomic and thermal parameters, and statistical parameters (the well-known compound $CaFe_2O_4$ was run on a Siemens D5000 diffractometer with poorer resolution, explaining the differences in refinement statistics). Fig. 3 shows typical refinement results. Regarding the occupation of iron and titanium on the two transition metal sites M1 and M2, no significant preference of titanium for either site was found. This is consistent with the situation in the $NaFeTiO_4$ end member, where previous studies concluded to a statistical distribution of iron and titanium [10].

$CaFe_2O_4$ and $NaFeTiO_4$ are expected to be stoichiometric [1–3]; this is confirmed by their colour, which is light brown for both compounds, in agreement with a strictly Fe^{3+} oxidation

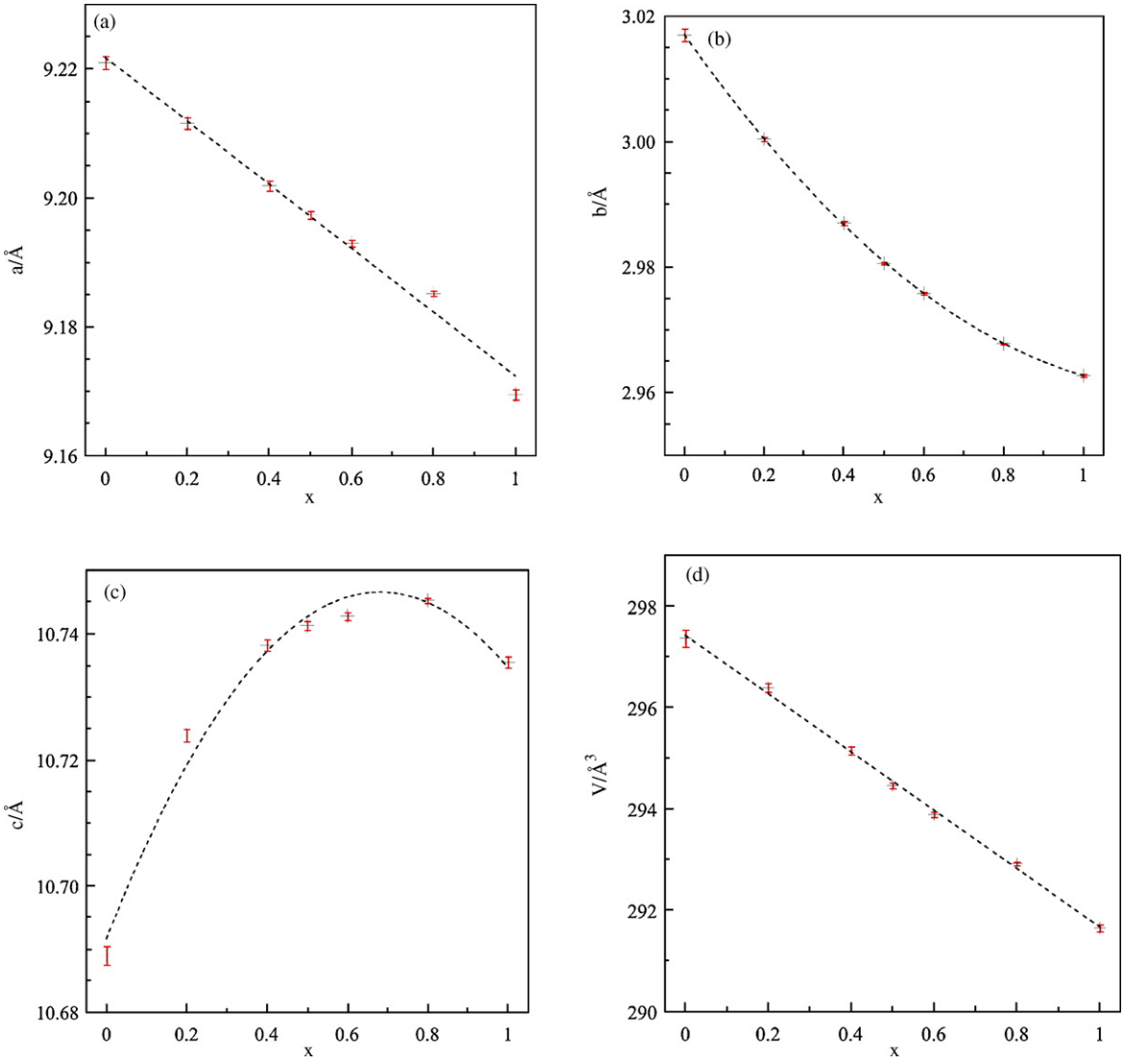

Fig. 2. Evolution of cell parameters (a–c) and of cell volume (d) throughout the $(Ca_{1-x}Na_x)(Fe_{2-x}Ti_x)O_4$ as a function of x. The lines are a guide to the eye.

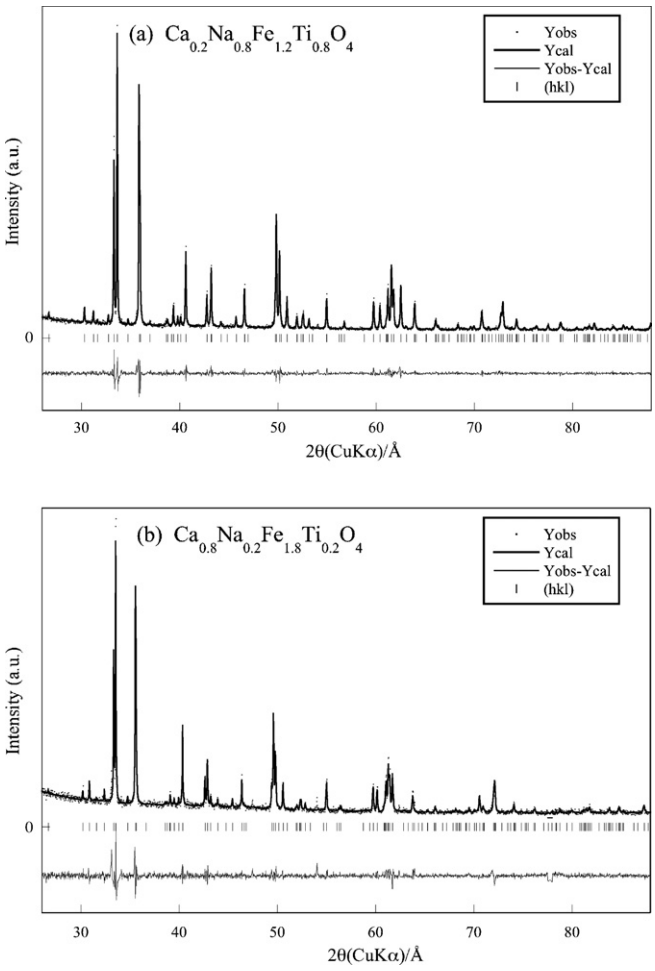

Fig. 3. Observed (points) and calculated (continuous line) X-ray powder diffraction patterns for (a) $x = 0.2$ and (b) $x = 0.8$. The lower part shows the difference $I_{obs} - I_{calc}$.

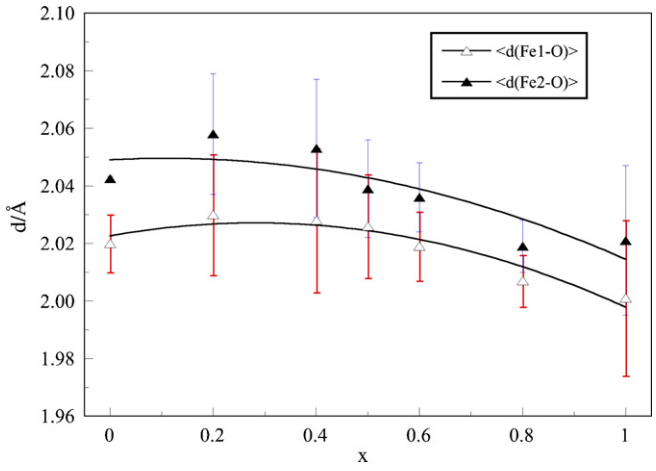

Fig. 4. Evolution of Fe(Ti)–O distances across the $(Ca_{1-x}Na_x)(Fe_{2-x}Ti_x)O_4$ solid solution. The lines are a guide to the eye.

state. High-temperature treatments, however, might introduce oxygen or sodium vacancies. This possibility was checked by refinements including variable occupations for sodium and the four oxygen positions; in all cases, the refined occupation factors were not significantly different from 1.

The evolution of distances and angles is given in Table 2. With increasing Na–Ti content, both Fe–O_1 and Fe–O_2 show a parallel evolution with a very slight bond length increase, followed by a decrease, as expected from the smaller Ti^{4+} ionic radius (see Fig. 4). In fact, consideration of average bond lengths is not very satisfying in this case, because of the rather irregular distribution of distances and angles around the Fe/Ti site (see Table 2). The evolution of the structure with composition may be better understood considering the Fe_1–O–Fe_2 octahedra pairs, which form the basic structural unit. As shown in Fig. 5, the Fe_1 bond to the linking oxygen O_1 decreases significantly with increasing x (from 2.03 to 1.90 Å), whereas the length of the other "arm" of this bridge, i.e. the Fe_2–O_1 bond, simultane-

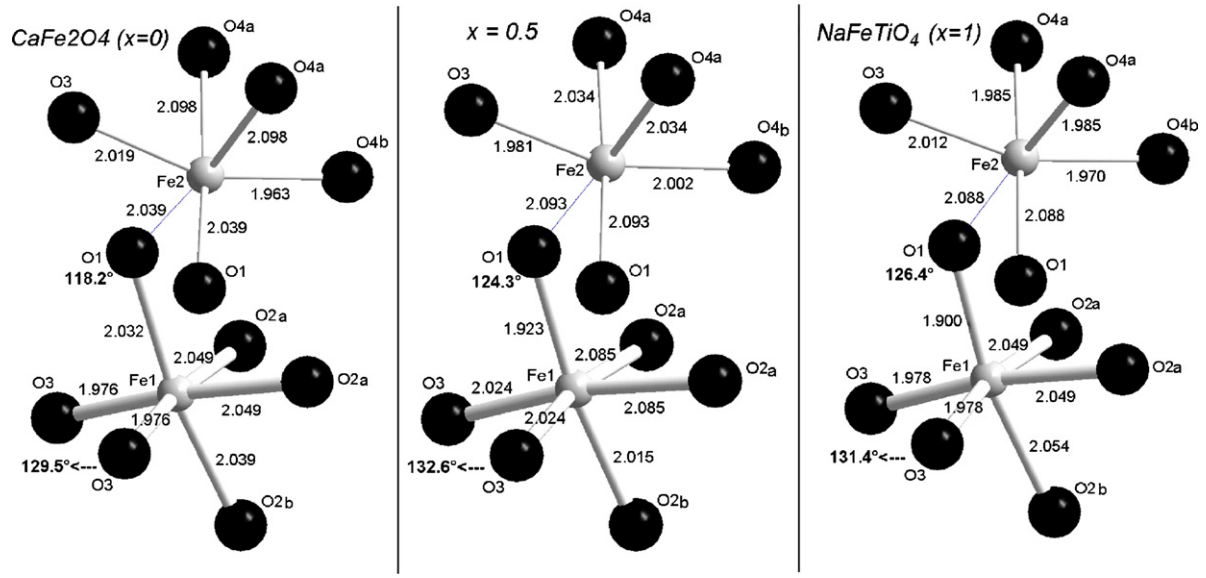

Fig. 5. Comparison of the iron and bridging oxygen environments for three compositions $x = 0$, 0.5 and 1.

Table 2
Evolution of Fe(Ti)–O distances along the $CaFe_2O_4$–$NaFeTiO_4$ solid solution

	x						
	0	0.2	0.4	0.5	0.6	0.8	1
Fe_1–O distances (Å)							
Fe_1–O_1	2.032 (14)	2.000 (27)	1.930 (32)	1.923 (23)	1.954 (2)	1.971 (12)	1.901 (33)
Fe_1–O_2 (×2) (a)	2.049 (9)	2.057 (19)	2.071 (23)	2.085 (17)	2.044 (11)	2.013 (8)	2.048 (24)
Fe_1–O_2 (b)	2.039 (13)	2.036 (26)	2.055 (30)	2.015 (22)	2.048 (15)	2.055 (11)	2.054 (31)
Fe_1–O_3 (×2)	1.976 (10)	2.014 (19)	2.020 (22)	2.024 (16)	2.012 (11)	1.994 (8)	1.978 (24)
⟨Fe_1–O⟩ (average)	2.020 (10)	2.030 (21)	2.028 (25)	2.026 (18)	2.019 (12)	2.007 (9)	2.001 (27)
σ^2(Fe_1–O) (Å^2)	0.00067	0.00048	0.00236	0.00191	0.00107	0.00067	0.00305
Fe_2–O distances (Å)							
Fe_2–O_1 (×2)	2.038 (10)	2.091 (19)	2.100 (22)	2.093 (16)	2.069 (11)	2.040 (8)	2.087 (23)
Fe_2–O_3	2.020 (15)	1.981 (28)	1.999 (32)	1.981 (23)	1.995 (16)	2.014 (12)	2.013 (36)
Fe_2–O_4 (×2) (a)	2.098 (11)	2.064 (18)	2.061 (21)	2.034 (15)	2.037 (10)	2.011 (8)	1.985 (22)
Fe_2–O_4 (b)	1.963 (14)	2.057 (25)	1.998 (29)	2.002 (21)	2.011 (14)	2.001 (11)	1.970 (29)
⟨Fe_2–O⟩ (average)	2.0425 (8)	2.058 (21)	2.053 (24)	2.039 (17)	2.036 (12)	2.019 (9)	2.021 (26)
σ^2(Fe_2–O) (Å^2)	0.00216	0.00136	0.00175	0.00177	0.00075	0.00026	0.00233
Fe–O–Fe angles (°)							
Fe_1–O_1–Fe_2	118.2 (7)	121.5 (1)	123.6 (1)	124.3 (9)	124.2 (6)	124.7 (5)	126.4 (1)
Fe_2–O_1–Fe_2	96.3 (5)	91.7 (8)	90.7 (9)	90.8 (6)	91.9 (4)	93.3 (3)	90.4 (9)
Fe_1–O_2–Fe_1	91.1 (5)	93.7 (8)	92.3 (9)	91.3 (6)	93.4 (5)	95.0 (4)	92.6 (9)
Fe_1–O_2–Fe_1	98.0 (6)	99.2 (1)	98.6 (1)	99.3 (9)	99.0 (6)	99.9 (5)	98.4 (1)
Fe_1–O_3–Fe_1	101.1 (5)	96.3 (8)	95.4 (9)	94.8 (6)	95.4 (4)	96.2 (3)	97.0 (9)
Fe_1–O_3–Fe_2	129.5 (7)	131.8 (1)	132.2 (1)	132.6 (9)	132.3 (6)	131.9 (5)	131.4 (2)
Fe_2–O_4–Fe_2	101.5 (6)	96.5 (9)	96.6 (1)	97.8 (8)	97.4 (6)	98.6 (4)	99.9 (1)
Fe_2–O_4–Fe_2	90.5 (5)	93.2 (7)	92.9 (8)	94.2 (6)	93.8 (4)	95.1 (3)	96.5 (9)

ously increases (from 2.039 to 2.088 Å). The bond angles also exhibit significant changes: values for the two bridging oxygen atoms O_1 and O_3 are indicated in Fig. 5, showing "breathing" of the bonds connecting the Fe_1 and Fe_2 edge-sharing octahedra with composition change. The Fe_1–O_3–Fe_2 angle, in particular, shows a maximum for $x = 0.5$–0.6, possibly connected with the odd variation of the c parameter.

3.2. Magnetic behaviour

The temperature dependence of the magnetization for various compositions is given in Fig. 6. The magnetization decreases with increasing Na–Ti content, in agreement with the dilution of the magnetic species Fe^{3+}. As expected for an ferrimagnetic material, the $CaFe_2O_4$ curve exhibits a wide anomaly below

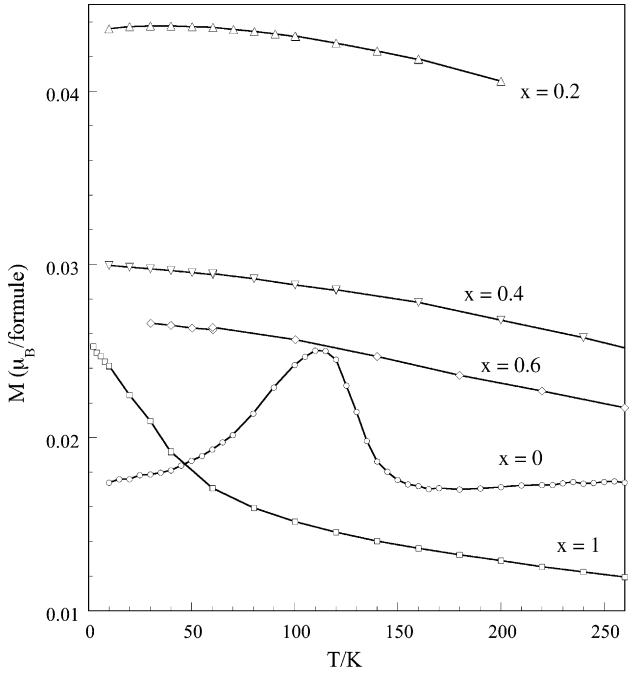

Fig. 6. Variation of magnetization of various $(Ca_{1-x}Na_x)(Fe_{2-x}Ti_x)O_4$ compositions as a function of temperature. Data measured in a 0.2 T applied field.

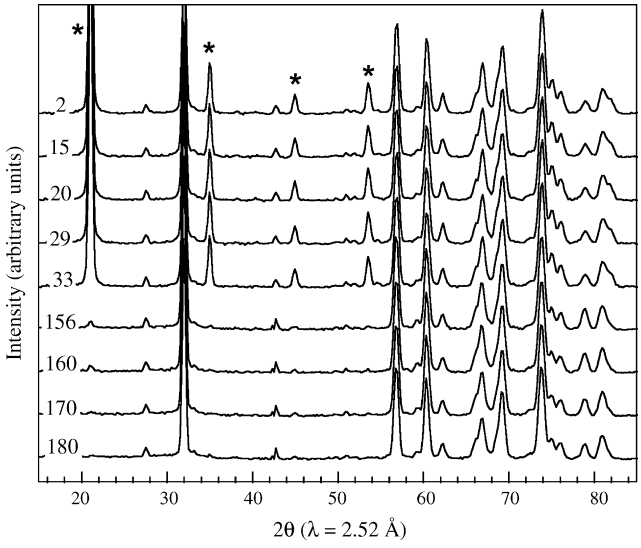

Fig. 7. Thermal evolution of the $CaFe_2O_4$ neutron diffraction pattern (measured at λ = 2.289 Å).

Table 3
Irreductible representations of the space group *Pnma* at point K [0 0 0]

Representation	$(2_x/½½0)$	$(2_y/0½½)$	$(\bar{1}/000)$	Eigen functions in the chemical unit cell		
				x	*y*	*z*
Γ_1	1	1	1			*C*
Γ_2	1	−1	1	*F*	*C*	
Γ_3	−1	1	1	*C*	*F*	
Γ_4	−1	−1	1			*F*
Γ_5	1	1	−1	*G*	*A*	
Γ_5	1	−1	−1			*A*
Γ_7	−1	1	−1			*G*
Γ_8	−1	−1	−1	*A*	*G*	

$T_C \approx 160$ K. Such a behaviour is clearly absent in all other samples, meaning that substitution of as little as 10% Fe by Ti (as for $x = 0.2$) completely suppresses antiferromagnetic ordering. So it seems that the long-range antiferromagnetic ordering between Fe_1 and Fe_2 spins is so sensitive to local magnetic exchange perturbations that it cannot take place when 10% Fe_1 and Fe_2 atoms are randomly substituted by a diamagnetic species.

3.3. Magnetic structure of $CaFe_2O_4$

Magnetic measurements showed the disappearance of antiferromagnetic ordering in all substituted $CaFe_2O_4$ samples. Consequently only unsubstituted $CaFe_2O_4$ was submitted to an X-ray and neutron thermodiffraction study. Low-temperature X-ray measurements showed that the crystal structure is unchanged on cooling down to 10 K.

The evolution of the neutron powder diffraction (NPD) pattern below $T_N = 160$ K is shown in Fig. 7. It shows the emergence of extra reflections below T_N, as well as intensity increases of other permitted reflections, indicating the onset of a magnetic ordering. All magnetic peaks can be indexed in the crystallographic unit cell, showing that the propagation vector *k* is equal to [0 0 0].

In order to solve the magnetic structure, the irreducible representations and the basis functions of each representation were calculated by applying the projection operator technique [11–13]

Table 4
Results of Rietveld refinements on $CaFe_2O_4$ XRD and neutron data at low temperature

	Cell parameters					
	X-rays (10 K)			Neutrons (2 K)		
	a (Å)	*b* (Å)	*c* (Å)	*a* (Å)	*b* (Å)	*c* (Å)
	9.218 (1)	3.0140 (4)	10.697 (2)	9.218[a]	3.014[a]	10.697[a]
	Positional parameters					
	X-rays (10 K)			Neutrons (2 K)		
	x	*y*	*z*	*x*	*y*	*z*
Ca	0.243 (4)	0.25	0.340 (3)	0.191 (11)	0.25	0.330 (10)
Fe_1	0.087 (3)	0.25	0.606 (2)	0.088 (5)	0.25	0.608 (3)
Fe_2	0.067 (3)	0.25	0.113 (2)	0.032 (7)	0.25	0.109 (4)
O_1	0.319 (8)	0.25	0.662 (8)	0.352 (5)	0.25	0.672 (9)
O_2	0.379 (7)	0.25	0.969 (7)	0.410 (7)	0.25	0.963 (8)
O_3	0.471 (9)	0.25	0.214 (7)	0.459 (8)	0.25	0.222 (11)
O_4	0.091 (8)	0.25	0.931 (7)	0.118 (6)	0.25	0.957 (11)
	Magnetic parameters					
	X-rays (10 K)			Neutrons (2 K)		
				$M(Fe_1)$	4.50 (39)	
				$M(Fe_2)$	−1.77 (32)	

Statistical parameters							
X-rays (10 K)					Neutrons (2 K)		
N (variables)	R_{wp}	R_{exp}	χ^2	R_{Bragg}	*N* (variables)	R_{wp}	χ^2
22	43.6	33.8	1.66	7.79	17	5.7	5.8

Space group *Pnma*.
[a] Not refined.

(see Table 3). The following modes were used for the two iron atom sites:

$$F = S_1 + S_2 + S_3 + S_4$$

$$G = S_1 - S_2 + S_3 - S_4$$

$$C = S_1 + S_2 - S_3 - \mathrm{S}_4$$

$$A = S_1 - S_2 - S_3 + S_4$$

All possible combinations of spins in the magnetic cell were tested against neutron powder diffraction data. The collinear representation Γ_4 gives the best agreement with the observed intensities and confirms that the magnetic moments are ordered in a (F_zF_z) spin arrangement. The results of X-ray and neutron refinements at low temperature are summarized in Table 4.

The z-component of the magnetic moments M_z are found to be $4.49\mu_B$ for Fe_1 and $-1.77\mu_B$ for Fe_2, resulting in a net magnetic moment of $2.72\mu_B$, to be compared with $2.22\mu_B$ obtained in the older study by Bertaut et al. [5].

4. Conclusions

We showed in this work that $CaFe_2O_4$ and $NaFeTiO_4$ form a continuous range of solid solution with simultaneous substitution of sodium for calcium and of titanium for half of iron. Titanium is distributed randomly on the two iron sites, within the accuracy of structural refinements. This double substitution results in subtle variations in bond lengths and angle, with an slight overall cell volume decrease with increasing Na–Ti content. The introduction of 10% titanium on iron sites is sufficient to prevent the onset of magnetic ordering. Finally, the crystal and magnetic structure of $CaFe_2O_4$ was checked using both X-ray and neutron diffraction at low temperature. The crystal structure is unchanged, and the ferrimagnetic structure proposed earlier by Bertaut et al. is confirmed.

References

[1] O. Muller, R. Roy, The Major Ternary Structural Families, Springer, Berlin, 1974, p. 55.
[2] T. Irifune, K. Fujino, E. Ohtani, Nature 349 (1991) 409–411.
[3] A.F. Reid, A.D. Wadsley, M.J. Sienko, Inorg. Chem. 7 (1968) 112–115.
[4] Y. Allain, B. Boucher, J. Phys. (Paris) 26 (1965) 789–792.
[5] E.F. Bertaut, J. Chappert, A. Apostolov, V. Semenov, Bull. Soc. Franç. Minéral. Cristallogr. 89 (1966) 206–212.
[6] P. Fertey, F. Sayetat, J. Appl. Crystallogr. 29 (1996) 692–699.
[7] J. Rodriguez-Carvajal, Phys. B. 55 (1993) 192–193.
[8] P. Wolfers, J. Appl. Crystallogr. 23 (1990) 554–557.
[9] R.D. Shannon, Acta Crystallogr. A32 (1976) 751–754.
[10] W.G. Mumme, A.F. Reid, Acta Crystallogr. B24 (1968) 625–631.
[11] E.F. Bertaut, Acta Crystallogr. A24 (1968) 217–222.
[12] C.J. Bradley, A.P. Cracknell, The Mathematical Theory of Symmetry in Solids, Clarendon Press, Oxford, 1972.
[13] S. Zouari, L. Ranno, A. Cheikh-Rouhou, O. Isnard, M. Pernet, P. Wolfers, P. Strobel, J. Alloys Compd. 353 (2003) 5.